Reactions of Aliphatic Alcohols on WO_3(001) Surfaces

S. Ma and B. G. Frederick*

Department of Chemistry and Laboratory for Surface Science and Technology (LASST) University of Maine, Orono, ME 04469

Received: May 19, 2003; In Final Form: August 21, 2003

Interactions of ethanol and 2-propanol with oxidized and reduced WO_3(001) thin film surfaces, grown epitaxially on a sapphire substrate, were studied with calibrated thermal desorption spectroscopy (CTDS). Coverage-dependent desorption spectra show that alcohol molecules diffuse rapidly on the WO_3 thin film surfaces. Ethanol and 2-propanol desorb molecularly between 200 and 450 K with evolution of water. The remaining alkoxy intermediates decompose via β-H elimination, followed by C−O bond scission, to produce ethylene and propylene, respectively. At low coverage, diffusion and competition between reaction rates of dehydroxylation vs associative molecular desorption of alcohol control the alkoxy coverage after the surface hydroxyls are depleted. The remaining alkoxy species undergo β-H elimination and C−O bond scission to produce the alkene. The selectivity toward alkene is controlled by surface reaction kinetics, rather than by surface structure.

I. Introduction

Understanding the surface reactivity of the WO_3 surface is of fundamental importance in exploring its potential applications. Tungsten oxide has been extensively studied as a catalyst in different forms. Oxide-supported WO_3 in the submonolayer uptake regime exhibits high catalytic activities for the metathesis reaction, olefin isomerization, and disproportionation reactions.[1−5] It has been used as the sensing element in detection of nitric oxides[6−8] and H_2S.[9−11] The properties of the crystalline WO_3 have been studied in detail, including its semiconductivity and production of oxygen vacancies and crystallographic shear (CS) planes.[12−18] However, the way in which the rate-limiting steps in specific surface reactions control the conductivity is not yet fully understood. In our laboratory, high quality WO_3 thin films have been fabricated,[19,20] and much effort has been focused on development of selective WO_3 thin film-based NO and organophosphorus compound sensors.[21,22]

In a previous publication, we have reported studies of the adsorption and desorption of methanol on WO_3 surfaces. Measurements were made on an oxidized surface and a reduced surface, characterized by XPS and UPS, to probe the structure dependence of the surface activity.[23] Our XPS and UPS data were compared to data in a single-crystal WO_3(001) study by Dixon et al. using XPS, UPS, and STM. This suggested that our oxidized surface was associated with the c(2×2) structure with line defects while the reduced surface was similar to the (1×1) structure with most of the surface terminal oxygens removed.[23,24] Our UPS measurements showed that methanol is molecularly adsorbed on the oxidized surface and dissociatively adsorbed on the reduced surface. The shape of the coverage-dependent desorption curves was modeled with Monte Carlo simulations, which imply that surface heterogeneity and facile surface diffusion are important during the desorption process. Formaldehyde and dimethyl ether, which are reaction products from defective TiO_2(001) surfaces,[25] were not detected.

We also studied the surface activity and reaction selectivity in the decomposition of dimethyl methylphosphonate (DMMP) on both surfaces.[26] The study showed that DMMP decomposes on both surfaces through production of methoxy intermediates. However, these two surfaces exhibited different reaction selectivity during decomposition of DMMP. Methanol and dimethyl ether were produced on the oxidized surface, but only dimethyl ether was observed on the reduced surface. Thus, in both the DMMP and methanol studies, the reduced and oxidized WO_3 surfaces behave differently. Such differences in activity toward carboxylic acids were also found on the oxidized and reduced surfaces of TiO_2 thin films.[27]

The surface activity is closely related to the surface structure. In WO_3, a crystalline network is formed from W−O−W chains in three dimensions, which can be described by corner-sharing octahedra. In comparison with the edge-sharing octahedral structures found in TiO_2, or face-sharing octahedral crystal structures, as in α-Al_2O_3, the corner-sharing octahedral structure results in a large spacing between metal cations. This leads to a large ($\approx$3.7 Å) separation between the Lewis base sites (the terminal oxygens) and Lewis acid sites (the coordinatively unsaturated tungsten cations) on the WO_3(001) surface. The large spacing may be responsible for the relatively poor activity toward dissociative adsorption of water and methanol on the oxidized WO_3(001) surface. The c(2×2) surface contains acid/base pairs required for dissociative adsorption, but the spatial separation between the acid/base sites also contributes to the activation energy barrier for extraction of the hydroxyl hydrogen.[23]

In this work we studied the reactions of ethanol and 2-propanol on these two WO_3 surfaces to further probe the surface activity and structure dependence of surface reactions. Tanner et al.[28] studied 1-propanol, 2-propanol, and *tert*-butyl alcohol on the oxidized single-crystal WO_3(001) surface. After desorption of the alcohols is nearly complete, dehydration to form alkenes is observed. The rate-limiting step in the alkene production was thought to be C−O bond scission. Although isopropoxide species were observed on the majority, Lewis

* Corresponding author. Tel: (207) 581-2268. Fax: (207) 581-2255. E-mail: brian.frederick@umit.maine.edu.

10.1021/jp035383c CCC: $25.00
Published on Web 10/08/2003

acid sites of c(2 × 2) terraces, the possible role of "minority defect sites" for dehydroxylation of the alcohol was mentioned. However, the factors that determine the alkoxy coverage and therefore the selectivity toward alkene remain unclear.

On TiO_2 surfaces, the coverage of alkoxy species remaining after evolution of the alcohol is complete is determined by the competition between associative desorption of alcohols and recombination of hydroxyls to form water.[29,30] Gamble et al.[30] proposed a defect-controlled model to explain the coverage of alkoxy species remaining on the TiO_2(110) surface. Using STM, Tanner et al.[28] identified adsorption of alkoxy species on the majority WO_3(001) terrace sites after the surface was annealed to temperatures where alcohol desorption is complete. There was no particular evidence for specific defect sites in controlling the selectivity toward the alkene. Thus, the CTDS data that we present here provide complementary information to distinguish the role of defects from that of diffusion and competitive desorption rates.

This study shows that the desorption of water and alcohols is shifted to higher temperature on the reduced WO_3(001) surface compared to the oxidized surface. The shape of the coverage-dependent desorption spectra indicates the importance of surface heterogeneity and relatively rapid diffusion of molecularly adsorbed alcohol, consistent with our previous observations for methanol on these two surfaces. During the CTDS experiments, removal of alcohols on the surface occurred through two channels: desorption of alcohol at lower temperatures and dehydration to alkene, which desorbed at higher temperature. The coverage dependence of the selectivity toward the alkene indicates that the alkoxy coverage remaining after dehydroxylation is controlled by the competition between surface reaction kinetics under the low coverage conditions of our experiments. We attribute the rate-limiting step in the ethanol dehydration reaction to C−O bond scission. Our data are not able to distinguish whether the β-H elimination or C−O bond scission is the rate-limiting step for 2-propanol dehydration. However, the comparison of *n*-propanol with 2-propanol in the study by Tanner et al.[28] indicates that C−O bond scission is again the rate-limiting step.

II. Experimental Section

All of the experiments were conducted in a stainless steel UHV chamber pumped by a turbo-molecular pump and an ion pump to a base pressure of 4×10^{-10} Torr. The design and structure of the system has been described previously in considerable detail.[31,23] In brief, this system was equipped with a differentially pumped quadrupole mass spectrometer, a sputtering gun, a concentric hemispherical electron energy analyzer, an Al/Mg Kα dual-anode X-ray source, and a differentially pumped ultraviolet (UV) lamp.

The calibrated thermal desorption spectrometer (CTDS) is designed for a sensitivity of 10^{-5} ML (1 ML is defined as 10^{15} molecules/cm^2) in a first-order desorption process. The time constant of the differential pumping system was designed to be 6 ms for N_2,[31] which was verified to be less than 100 ms in its response to methanol.[23] For calibration of the mass spectrometer, gas was released from a known volume gas cell through a positive shutoff valve that acts as an effusion source into a microchannel array doser. The doser provides a flow rate comparable to that in thermal desorption experiments.[31] The pressure in the gas cell was monitored by a spinning rotor gauge, which has an absolute accuracy of 3% over the 10^{-7} to 10^{-1} mbar pressure range.[31] The mass spectrometer current was measured with a Burr-Brown board, modified to operate as an auto-scaling amplifier. In calibration experiments, the mass spectrometer current as a function of the flow rate was linear over 3 orders of magnitude. With this design, the mass spectrometer current can be calibrated against the known flow of inert gas leaving the gas cell. The doser was translated with respect to the aperture in the shroud of the differentially pumped mass spectrometer to quantify the flux distribution of the doser and transmission of the entrance aperture.[31] During a desorption experiment, the sample is placed within 1 mm of the aperture in the mass spectrometer shroud. Hence, the surface coverage can be calculated directly from the known flow calibration, rather than by reference to an assumed coverage of a known single-crystal adsorption structure. This alleviates the problem of calibration for surfaces that are not ordered structures on a single crystal. An independent estimate of the absolute accuracy of the CTDS system was obtained from measurements of the saturation coverage of oxygen in the c(2 × 4) structure on Pd(110).[31] The results were within 12% of measurements reported utilizing nuclear activation analysis.[31]

For compounds that stick to the doser and vacuum system walls, such as alcohols, more complex procedures for calibration of the mass spectrometer current were performed using a second spinning rotor gauge mounted in the main chamber. The calibration procedures were described previously.[23] The flux impinging on the entrance aperture of the mass spectrometer shroud is given by the kinetic theory of gases as $\Gamma = P/\sqrt{2\pi mkT}$. At the pressures utilized here, this is a valid approximation. The multiplier current is proportional to the flux; i.e., $I^{SEM} = c\Gamma$. To allow for degredation of the multiplier over time, we define $I^{SEM} = I^F \cdot G$, and distinguish the current measured with the Faraday plate, I^F, from G, the SEM gain. Thus, the calibration factor, $c = (I^F/P)G\sqrt{2\pi mkT_{cal}}$, for a given mass fragment (at the chamber calibration temperature T_{cal}), includes the pumping speed through the ionizer (at the calibration temperature), the ionization cross section, and the mass spectrometer's transmission efficiency. Our error analysis showed that the uncertainty in surface coverage was below 30% for very low coverage and below 20% for high coverage.

Growth, mounting, and cleaning of the WO_3 thin film sample was described in a previous paper.[23] The 500 Å epitaxial WO_3 thin film was grown at a rate of 1Å/s on the r-cut sapphire substrate held at 773 K. Films were deposited using RF magnetron sputtering of a pure tungsten target in a 50/50 argon and oxygen ambient at a total pressure of 3 mTorr. The sample was mounted onto a tantalum block, which was resistively heated to 800 K, and cooled to 140 K via Ta wires. A K-type thermocouple, spot-welded on the back of the tantalum block, was used to control the surface temperature. In calibration experiments afterward, a thermocouple was attached to the front face of the film with ceramic adhesive (Ceramabond). Near 300 K, the temperature of the front face was similar to the back, but at 500 K it was lower by 25 K, and at 600 K it was nearly 50 K lower. The characterization of the thin film has been reported previously.[19,32]

The WO_3 thin film surface was cleaned before adsorption experiments by Ar^+ sputtering (100 μA beam current and 500 eV beam energy) at a pressure of 1.0×10^{-4} Torr, primarily to remove carbon. The reduced surface for these experiments was produced by heating the sputtered surface at 4 K/s to 800 K for several cycles until no desorption products were observed. The oxidized surface was made by heating the sputtered surface in 0.24 mbar oxygen at 300 °C for 2 h, as described previously.[23] The XPS and UPS data given previously[23] characterize the distribution of W^{6+} and W^{5+} sites on the surfaces studied here.

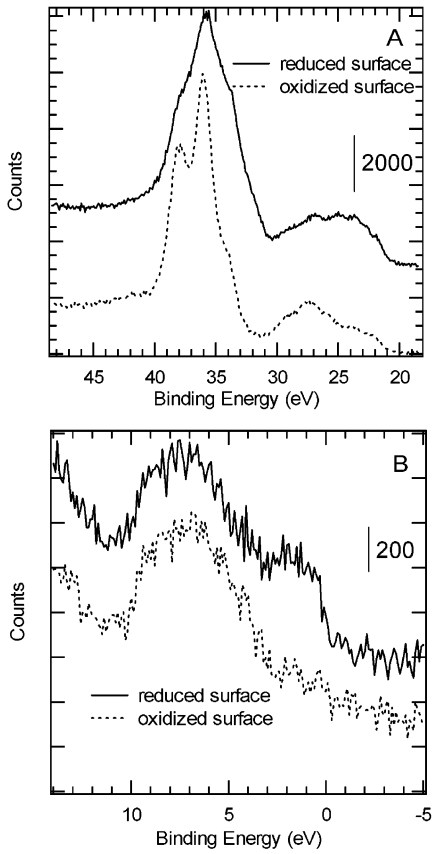

Figure 1. XPS spectra for the reduced and oxidized WO_3 thin film surfaces used for 2-propanol CTDS experiments. (A) W4f band, and (B) valence band.

For completeness, Figure 1 shows the XPS spectra for the reduced and oxidized WO_3 thin film surfaces that were used for the 2-propanol adsorption and desorption experiments. Similar spectra were obtained for the reduced and oxidized WO_3 thin film surfaces used for the ethanol and water desorption experiments. Figure 1A shows the W4f band and the valence band regions are given in Figure 1B. Compared to the oxidized surface, the reduced surface has a significant increase in the density of states in the gap near the Fermi level and a decrease in the intensity of the O2p band. The W4f doublet due to spin−orbit splitting cannot be resolved for the reduced surface. The change in the surface electronic structure for the reduced surface is ascribed to the preferential sputtering of lattice oxygen, resulting in formation of oxygen vacancies.

The coverage-dependent desorption spectra that will be shown for each adsorbate were performed sequentially on a single surface preparation. In separate experiments, we checked the reproducibility of the peak positions and found no effects of surface reduction on the desorption spectra. We note that XPS results did not show evidence of additional surface reduction after desorption of the alcohols, as indicated by the W4f band, perhaps due to the extremely high oxygen vacancy diffusion rates in WO_3.

Ethanol (Aldrich >99.5%) and 2-propanol (Aldrich 99.5%) were further treated by freeze−pump−thaw cycles, and their purity was checked using the mass spectrometer before dosing onto the WO_3 thin film surfaces. Mass spectra for ethanol and 2-propanol show a negligible amount of water in both samples.

The Monte Carlo simulation method was presented in our previous paper in detail.[23] Briefly, the adsorption energy of each site was chosen from a random distribution. The lattice was then populated randomly with adsorbates. The surface heterogeneity and interactions between adsorbates contributed to the probability of both desorption and surface diffusion attempts, which were treated as competitive processes in each time step. Initial simulations utilized lattices with 100×100 sites, but larger, 200×200 lattice sizes were then used for production runs. The time step was varied between 0.1 and 0.5 s to test convergence of the algorithm. For $\Delta t \geq 0.5$ s, significant peak shifts were observed; therefore, a time step of $\Delta t = 0.2$ s was utilized for the spectra shown. Comparisons were also made to direct numerical solution of the corresponding Polanyi−Wigner equation for the rapid diffusion limit.

III. Results

III.A. Ethanol Interaction with the Reduced WO_3 Surface. A set of coverage-dependent desorption spectra on the reduced surface are shown in Figure 2. As the surface coverage decreased, the desorption temperature increased. On the basis of our Monte Carlo simulations,[23] diffusion is sufficiently rapid that molecules migrate to and desorb from the most stable adsorption sites. For a coverage of 0.012 ML, ethanol desorption was observed at 432 K on the reduced WO_3 surface. Adsorption of the first layer saturated at a coverage slightly greater than 0.63 ML and a multilayer desorption peak appeared at 165 K for a coverage of 0.72 ML. The characteristics of the overlapping leading edge and the increase of the peak temperature with coverage are consistent with zeroth order desorption kinetics for multilayer desorption, with a desorption energy of 47 kJ/mol. At an ethanol surface coverage greater than 0.18 ML, an additional high-temperature desorption peak, in the expanded spectra of Figure 2A, emerged at 650 K. This coincides with ethylene desorption, as shown in Figure 2B (described below).

During the ethanol CTDS experiment on the reduced surface, ethylene was produced from ethanol dehydration and detected around 650 K. Since masses 26, 27, and 28 are the major fragments of ethylene, as well as fragments of ethanol, the desorption of ethylene is superimposed on the ethanol desorption spectrum and cannot be distinguished from ethanol desorption directly. However, the ethylene fragmentation pattern does not contain mass 31, which is the strongest ion in the ethanol fragmentation pattern. By scaling the mass 31 desorption trace based on the fragmentation pattern of ethanol, the ethanol contribution to masses 26, 27, and 28 was removed from these spectra. The resulting ethylene desorption spectra for 27 amu are shown in Figure 2B. Note that ethylene production increases with the surface coverage of ethanol, but the desorption temperature is constant.

In Figure 2C, the corresponding water desorption spectra (mass 18) are presented. As the ethanol coverage increased to 0.034 ML, water desorption was observed at 350 K and the desorption temperature decreased with increasing ethanol coverage. The low-temperature water peaks are similar to spectra (see section III.E) for adsorption of water. Very weak water desorption was detected above 700 K, which increased in intensity with the ethanol coverage.

III.B. Ethanol Interaction with the Oxidized WO_3 Thin Film Surface. The ethanol CTDS data for the oxidized WO_3 surface are presented in Figure 3 in a manner similar to Figure 2, with the contributions due to ethanol, ethylene, and water in parts A, B, and C, respectively. As the surface coverage decreases, again the desorption temperature increases. Ethanol desorbs at 418 K for a surface coverage of 0.0024 ML. In comparison with the spectra of Figure 2A, the desorption temperature on the oxidized surface is lower than on the reduced

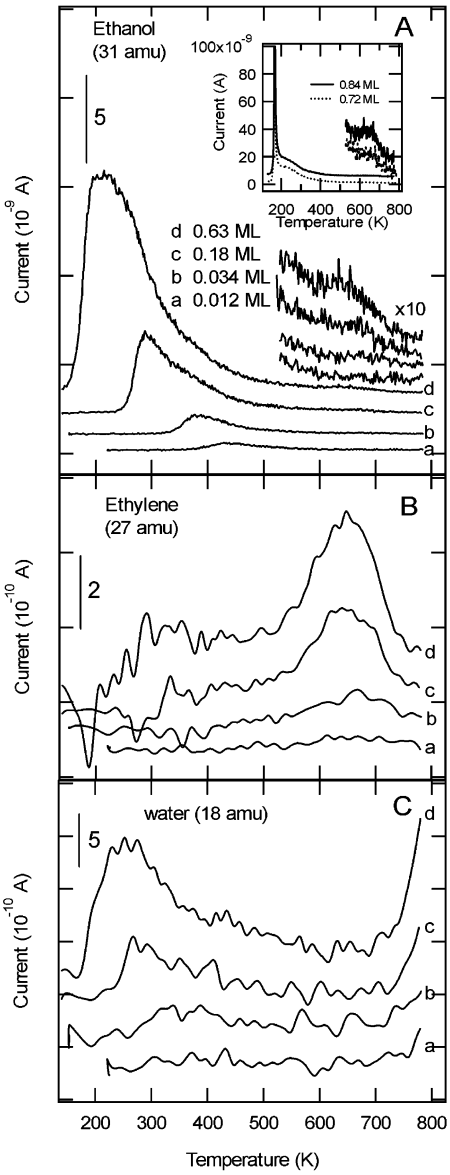

Figure 2. Ethanol reactions on the reduced WO_3 thin film surface. (A) Ethanol molecular desorption spectra presented as mass 31 for different coverages. The high-temperature portion of the desorption spectra were expanded as indicated. (B) The corresponding ethylene desorption spectra, shown as mass 27, which coincided with the high-temperature ethanol desorption peak. Spectra were obtained by removing the contribution from ethanol (see text for details). (C) The corresponding water desorption spectra. The reduced WO_3 thin film surface was produced by Ar^+ sputtering (500 eV, 100 μA beam current, 110 s). Dose was conducted at low temperature and the ramp rate was 4 K/s. Peaks were offset for clarity. Note that the tails on the high-temperature side of the alcohol spectra overlap in the original data. (The same is true for all of the alcohol spectra presented in Figures 3A, 5A, 6A, and 7A.)

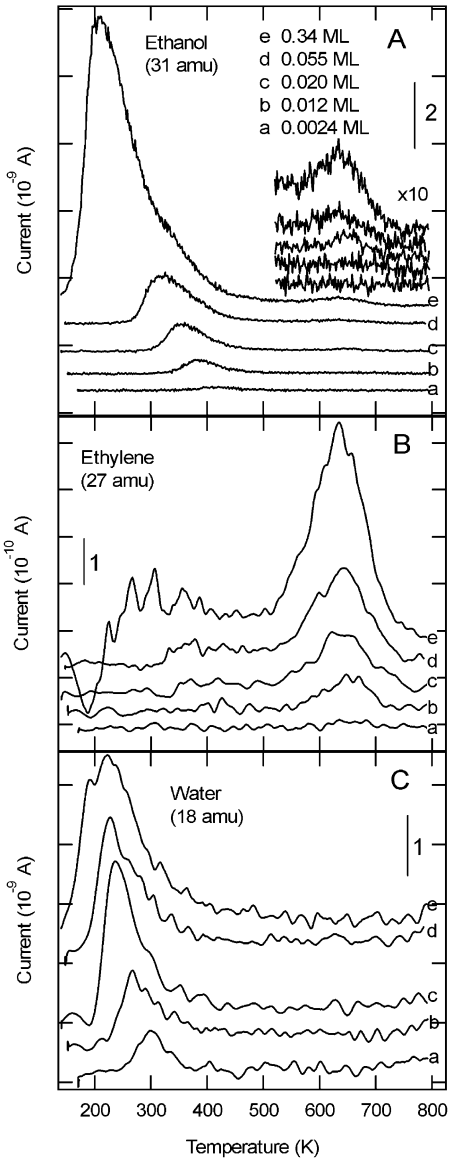

Figure 3. Ethanol reactions on the oxidized WO_3 thin film surface. (A) Ethanol molecular desorption spectra presented as mass 31 for different coverages. (B) The corresponding ethylene desorption spectra (mass 27), and (C) water desorption spectra presented as in Figure 2. The oxidized WO_3 thin film surface was produced by oxidizing the reduced surface in 0.24 mbar O_2 at 300 °C for 2 h. Dosing was conducted at low temperature and the ramp rate was 4 K/s. Peaks were offset for clarity.

surface at the same coverage and the peak shape is skewed to lower temperature. The difference in desorption temperatures as a function of the absolute coverage is quantified in Figure 4. On the basis of our Monte Carlo simulations of methanol, these spectra suggest a skewed distribution of adsorption site energies with a smaller population at higher adsorption energy. At coverages greater than 0.02 ML, an ethanol desorption peak is observed above 600 K, which overlaps with the ethylene desorption peaks (Figure 3B), as on the reduced surface. The intensity of the desorption peak increases with ethanol surface coverage, as shown by the expanded spectra in Figure 3A.

Ethylene desorption was detected near 650 K for a surface coverage greater than 0.0024 ML. As in the case of the reduced WO_3 surface, the ethylene desorption peaks do not shift with coverage. The corresponding water desorption spectra are shown in Figure 3C. For an ethanol coverage of 0.0024 ML, water desorption was detected at 295 K. The desorption temperature decreases with increasing surface coverage, similarly to the low temperature water desorption profiles on the oxidized surface (discussed in section III.E). However, compared to the ethanol reaction on the reduced surface (Figure 2C), desorption of water above 700 K was dramatically reduced.

III.C. 2-Propanol Interaction with the Reduced WO_3 Surface. During 2-propanol CTDS experiments on the reduced WO_3 surface, desorption of 2-propanol, propylene, and water were observed, which is shown in Figure 5A, B, and C, respectively. The 2-propanol and propylene desorption overlap around 500 K (Figure 5A and 5B). Propylene has major

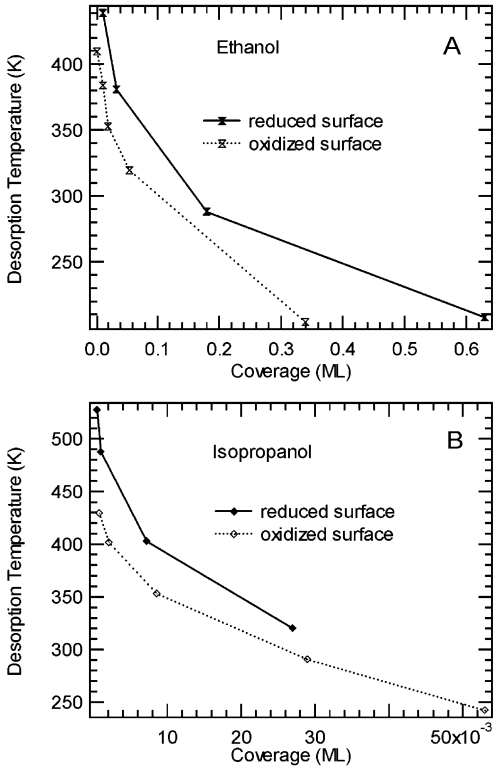

Figure 4. Plots of the peak desorption temperature as a function of surface coverage for (A) ethanol and (B) 2-propanol in CTDS experiments on both the reduced and oxidized WO_3 thin film surfaces. The desorption temperature on the reduced surface is consistently higher than on the oxidized surface.

fragments at masses 39, 41, and 42, which are also cracking fragments of 2-propanol, but does not have the mass 45 fragment, which is the dominant fragment of 2-propanol. Therefore, the propylene desorption spectrum (Figure 5B), was obtained by subtraction of the 2-propanol contribution to mass 41 by scaling the mass 45 trace according to the 2-propanol fragmentation pattern. 2-Propanol desorption appeared at 530 K for a surface coverage of 0.00045 ML; the desorption temperature decreased as the surface coverage increased. As in the case of ethanol, the coverage-dependent behavior suggests that 2-propanol diffusion is sufficiently fast that the molecules find the stronger binding sites.[23] Multilayer desorption was detected at 175 K, as shown in the inset of Figure 5A, with characteristic zeroth order desorption and a desorption energy of 27 kJ/mol. In comparison with ethanol CTDS, the 2-propanol molecular desorption peak occurs approximately 100 K higher, but no high-temperature, recombinative desorption peak was detected. The higher desorption temperature for 2-propanol with respect to ethanol is consistent with the higher molecular weight. At a total coverage less than 0.00045 ML, 2-propanol desorption was not detected, but propylene was still observed at 527 K. The production of propylene increases with the 2-propanol surface coverage, with a peak position independent of coverage, but at a substantially lower temperature than the ethylene peak at 650 K observed for ethanol dehydration.

A broad water desorption peak was observed around 400 K as the surface 2-propanol coverage increased to 0.0072 ML. Note that propylene was already detected at lower 2-propanol exposures. This water desorption profile evolved into two desorption peaks centered at 317 and 508 K, for a 2-propanol coverage of 0.027 ML (Figure 5C). The position of the lower-temperature peak decreased with increasing surface coverage, similar to the behavior following water adsorption on the

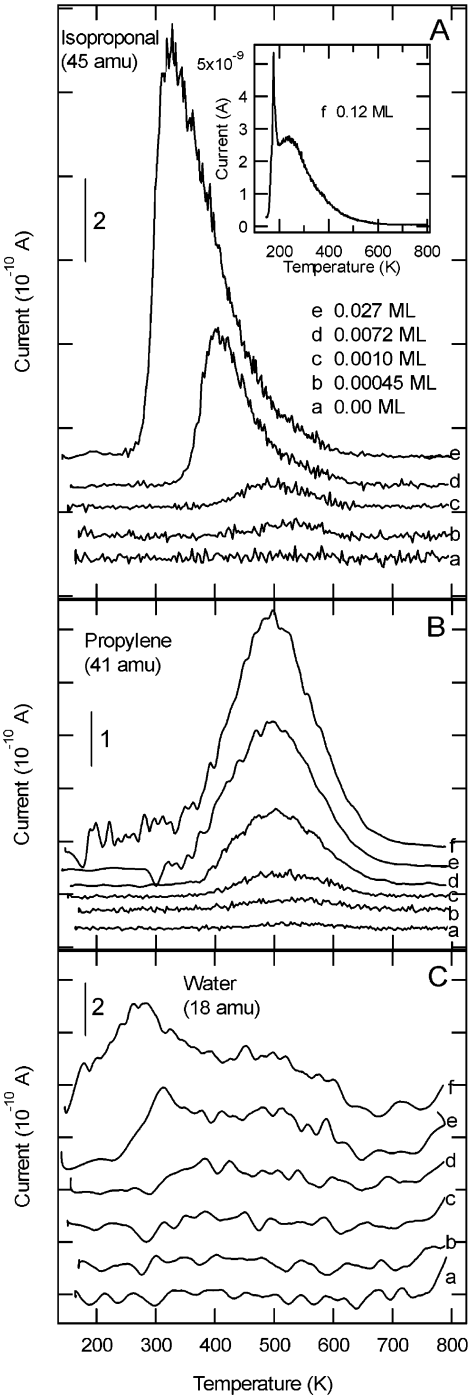

Figure 5. 2-Propanol reactions on the reduced WO_3 thin film surface. (A) 2-Propanol molecular desorption spectra presented as mass 45 for different coverages, with the multilayer desorption of 2-propanol presented in the inset. (B) The corresponding propylene desorption spectra (mass 41), obtained by removing the contribution from 2-propanol (see text for details), and (C) water desorption spectra with two desorption peaks resolved at high 2-propanol coverages. The reduced WO_3 thin film surface was produced by Ar^+ sputtering (500 eV, 100 μA beam current, 110 s). Dose was conducted at low temperature and the ramp rate was 4 K/s. Peaks were offset for clarity.

reduced surface (section III.E). Note that the broad, higher-temperature desorption peak, shown in curves e and f of Figure 5C, overlaps with the desorption of propylene and that the peak position is relatively coverage independent. The water desorption above 700 K, which was detected for ethanol on the reduced surface, was suppressed.

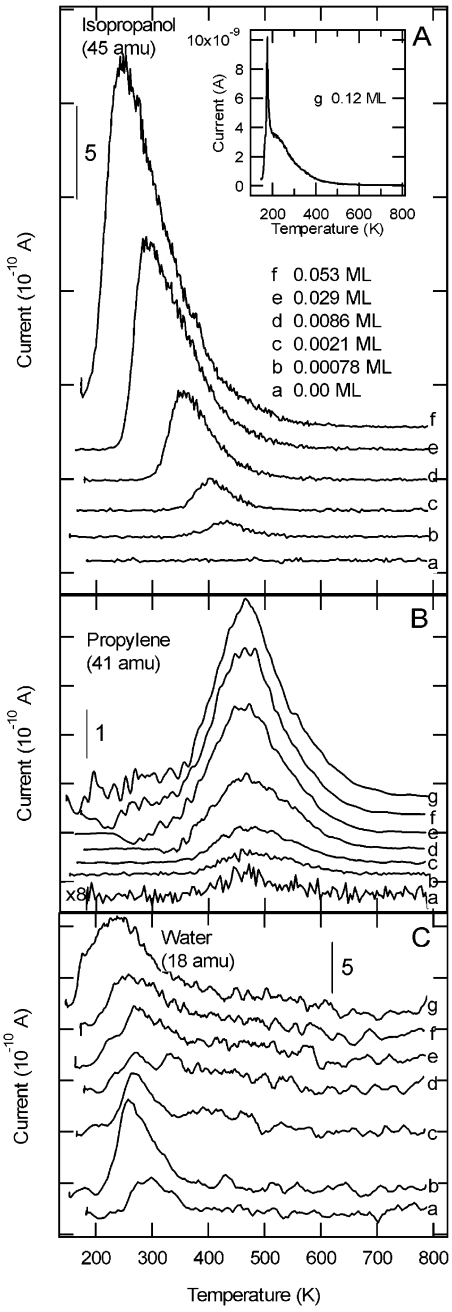

Figure 6. 2-Propanol reactions on the oxidized WO_3 thin film surface. (A) 2-Propanol molecular desorption spectra presented as mass 45 for different coverages. (B) The corresponding propylene desorption spectra (mass 41), and (C) water desorption spectra as described in Figure 5. The oxidized WO_3 thin film surface was produced by oxidizing the reduced surface in 0.24 mbar O_2 at 300 °C for 2 h. Dosing was conducted at low temperature and the ramp rate was 4 K/s. Peaks were offset for clarity.

III.D. 2-Propanol Interaction with the Oxidized WO_3 Surface. The 2-propanol dehydration reaction also occurred on the oxidized WO_3 surface. Figure 6 shows the desorption spectra for 2-propanol, and the corresponding propylene and water desorption spectra. The propylene spectra (Figure 6B), were obtained by subtraction of the 2-propanol contribution as described for the reduced surface. Again, the 2-propanol spectra overlapped with propylene desorption above 400 K.

At a 2-propanol coverage of 0.00078 ML, desorption was observed at 433 K, which was about 100 K lower than on the reduced surface, as shown in Figure 4B. The desorption temperature increased with decreasing surface coverage, which implies that 2-propanol diffusion is relatively rapid compared to desorption.[23] Similarly to the reduced WO_3 surface, only one 2-propanol desorption peak was observed. For a surface coverage less than 0.00078 ML, 2-propanol desorption was not observed; however, very weak propylene desorption was detected at 467 K (Figure 6B, curve a). The production of propylene increased with 2-propanol surface coverage, but the desorption temperature did not change. By contrast to the ethanol results, the desorption temperature of the dehydration product was significantly lower on the oxidized surface than on the reduced surface. A multilayer desorption peak at 175 K appeared at a coverage of 0.12 ML (inset of Figure 6A). The desorption energy of 27.4 kJ/mol is essentially identical to the multilayer desorption energy on the reduced surface.

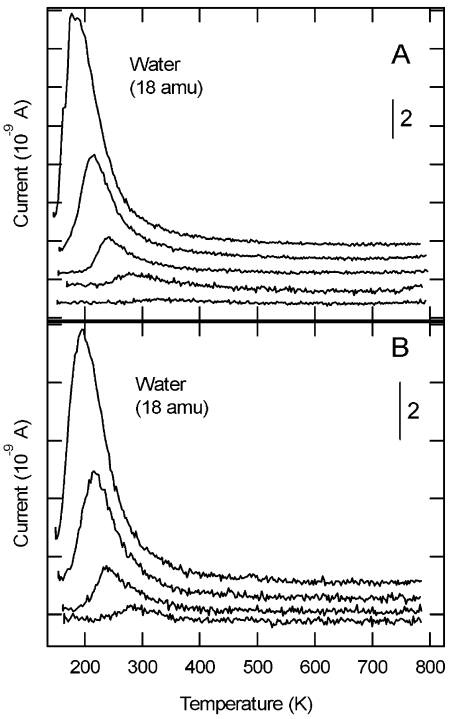

Figure 7. Water thermal desorption spectra at different coverages: (A) on the reduced WO_3 thin film surfaces and (B) on the oxidized WO_3 thin film surface. The conditions for producing these surfaces and measuring the thermal desorption spectra were similar to those used in the alcohol experiments.

The water desorption spectra exhibited different features on the oxidized surface than those on the reduced surface. At a coverage less than 0.00078 ML, water desorption was detected at 298 K, which was observed on the reduced surface only at high 2-propanol coverage. The desorption temperature for this state decreased as the surface coverage increased, as found for molecular adsorption (see section III.E). As the 2-propanol surface coverage increased to 0.0021 ML, a very weak desorption peak appeared around 405 K. With further increases in coverage, this desorption peak broadened (Figure 6C curves d−g) and overlapped with the desorption of propylene. On the oxidized WO_3 surface, some water desorption due to background adsorption was found below 350 K. Therefore, the spectra for water below 350 K includes contributions from both dissociative adsorption of alcohol leading to dehydroxylation and condensation of background water vapor, which was introduced into the chamber during oxidation of the WO_3 surface.

During the ethanol and 2-propanol CTDS experiments, dehydrogenation reaction products, such as acetaldehyde and acetone, were not detected. This indicates that the WO_3 thin film surface exhibits only dehydration activity.

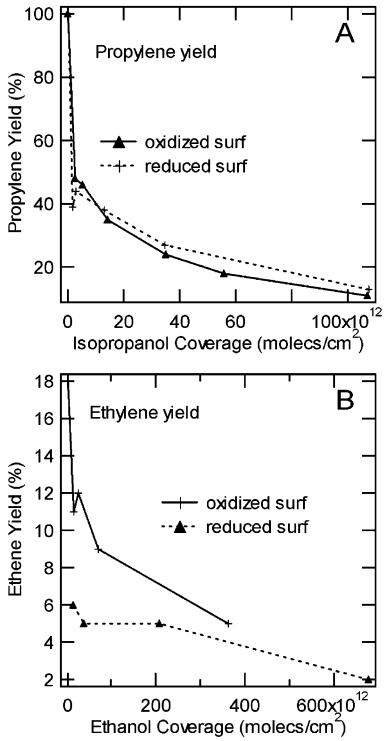

Figure 8. Comparison of the yield of alkene dehydration products from (A) propylene and (B) ethylene on the oxidized and the reduced WO_3 surfaces, plotted as the ratio of integrated ion current vs alcohol coverage. (see text for details.)

III.E. Water Adsorption and Desorption on the Reduced and Oxidized WO_3 Surfaces. Water adsorption and desorption was also studied in order to understand the surface dehydration reaction of ethanol and 2-propanol on the WO_3 surfaces. Water desorption spectra are displayed in Figure 7A for the reduced WO_3 surface and in Figure 7B for the oxidized WO_3 surface. The peak desorption temperature decreased as the surface coverage increased on both surfaces. On the reduced surface the desorption temperature was higher than that on the oxidized surface, similar to the behavior for the alcohols (not shown).

III.F. Relative Yield of Dehydration Products on the WO_3 Surfaces. Figure 8 shows the yield of ethylene and propylene during the dehydration of ethanol and 2-propanol, respectively, on both the reduced and oxidized WO_3 surfaces. The plot is simply the ratio of the integrated ion currents ([ethylene/(ethylene + ethanol)] and [propylene/(propylene + 2-propanol)]) without correcting for their respective calibration factors. In fact, the ratios of the relative ionization probabilities for the alcohols to those of their corresponding alkenes are both approximately 1.5.[33−35] Therefore, correcting the area ratios will not qualitatively change the plot. As shown in Figure 8, the yields of ethylene and propylene were strongly coverage dependent, but were not significantly different for the oxidized vs the reduced WO_3(001) surfaces, demonstrating the insensitivity of the dehydration of alcohols to the surface structure.

IV. Discussion

We first examine the mechanism of the dehydration reaction and identify the rate-limiting step as C−O bond scission. We assume that the dehydration product evolves from alkoxy species remaining on the surface after the low-temperature desorption of the alcohol is complete, and therefore the alkoxy coverage determines the selectivity toward the alkene. We then consider two models to understand how the selectivity, i.e., the ratio of the alkene to alcohol, is controlled in the thermal desorption process. A particularly thorough study of the role of surface defects in the dehydration of alcohol on the TiO_2(110) surface was published by Gamble et al.[30] using isotope labeling techniques. In our analysis of alcohol dehydration on the WO_3 thin film surfaces we first consider whether a defect model controls selectivity, largely in comparison with the results obtained on the TiO_2(110) surface.[30] We then suggest that on WO_3(001) surfaces, a model involving diffusion and relative reaction rates is more important, at least under the low coverage conditions of our study.

IV.A. Mechanism of Dehydration Reactions. On both the oxidized and the reduced WO_3 surfaces, the ethylene desorption temperature, detected above 600 K (Figures 2B and 3B), is higher than the propylene desorption temperature, observed between 400 and 600 K (Figures 5B and 6B). Our observations are consistent with the observations for alcohol dehydration reactions on the TiO_2(001) surface by Kim and Barteau.[36] In both cases, the larger alkene desorbs at lower temperature, suggesting that desorption of the dehydration products is reaction limited, rather than desorption limited. The coverage independence of the desorption temperatures for ethylene and propylene on our heterogeneous WO_3 surfaces also supports this conclusion. The study by Tanner et al.[28] of the dehydration reactions of 1-propanol and 2-propanol on the single-crystal WO_3(001) surface showed that propylene is produced at a lower temperature from 2-propanol than from 1-propanol.

Dehydration of the alkoxy species requires cleavage of either the α- or β-CH bond, and C−O bond scission. We now consider whether each of these is the rate-limiting step. Generally, the α-H bond is more acidic than the β-H, because the former C−H bond is more polarized by the oxygen atom. Several studies have shown that α-H abstraction results in formation of aldehydes or ketones for alcohols on oxide surfaces.[29,36−40] However, acetaldehyde and acetone were not detected during our experiments with ethanol and 2-propanol, respectively, on the WO_3 surfaces. Using isotope labeling techniques, Gamble et al.[30] have determined that, for ethoxy species on the TiO_2(110) surface, α-H abstraction and subsequent H migration during the dehydration reaction can be ruled out. Therefore, α-H abstraction of the alcohols on the WO_3 surfaces seems unlikely.

If abstraction of the β-H is the rate-limiting step, ethylene and propylene would be formed at similar temperatures. The energy barriers for breaking the β-CH bonds in ethanol and in 2-propanol should be similar due to the similarity in their local chemical structures and adsorption configurations on the surfaces. In this case, for a reaction limited surface process, desorption of ethylene and propylene should occur at similar temperatures, which contradicts our observations.

We conclude that cleavage of the C−O bond is the most likely rate-limiting step for the dehydration reaction of ethanol, but not necessarily 2-propanol, on the WO_3(001) surfaces. This can be justified on the basis that the stability of the carbocation intermediate, produced by breaking the C−O bond, decreases in the order tertiary > secondary > primary, as suggested by Tanner et al.[28] for their comparison of *n*-propanol, 2-propanol, and *tert*-butyl alcohol dehydration. To the extent that the energy barrier height decreases with increasing stability of the carbocation formed, C−O bond scission in 2-propanol should occur at a lower temperature than in ethanol, and produce propylene at a lower temperature than ethylene. This trend is consistent with our data as well as that of Tanner et al.[28] and of Kim and Barteau.[36]

Gamble et al.[30] identify β-H elimination from one ethoxy species on the $TiO_2(110)$ as the rate-limiting step which produces the proton for associative desorption of coadsorbed ethoxy species to produce ethanol. However, they suggest that the delay in the ethylene desorption peak, relative to the ethanol peak, is due to a somewhat higher barrier for cleavage of the C−O bond in the $-OCH_2CH_2-$ species. A similar, though small, temperature shift between the ethanol and ethylene peaks can also be observed in our experiments on the WO_3 surfaces in Figures 2 and 3. This implies that *breaking the C−O bond is the rate-limiting step for ethylene production*.

Figures 5 and 6 show that propylene desorption is accompanied with water desorption. This water desorption temperature is higher than that found in water adsorption experiments and is clearly resolved from the low-temperature desorption peak, assigned to recombination of surface hydroxyls formed during dissociative adsorption of 2-propanol. We attribute it to the recombination of surface hydroxyls resulting from abstraction of the β-H from isopropoxy on the surfaces. However, because of the similarity in the desorption temperatures for water and propylene, the barriers to C−O bond scission and β-H elimination may be similar.

IV.B. Selectivity toward Alkene Production. Our experiments show that two channels are available for removal of adsorbed ethanol and 2-propanol: desorption as alcohol molecules and desorption as alkenes via dehydration reactions. We present two limiting cases that potentially control the selectivity of one channel vs the other. The first is based upon recent work on other oxide single-crystal surfaces in which the yield of alkene is determined by particular surface defect sites; the second is based upon the role of diffusion rates and reaction kinetics, without necessarily requiring "special" defect sites. We then discuss the experimental evidence and conclude that, under the low coverage conditions of our experiments, the second model controls the selectivity to alkenes.

In either case, the adsorption of the alcohol may be (1) associative, (2) dissociative, or a mixture of alcohol and alkoxy species:

$$\mathrm{ROH(g)} \rightarrow \mathrm{ROH(a)} \quad (1)$$

$$\mathrm{ROH(g)} + \mathrm{O(l)} \rightarrow \mathrm{RO(a)} + \mathrm{H...O(l)} \quad (2)$$

where "g" is for the species in gas phase, "a" for the species adsorbed on surface, and O(*l*) represents lattice oxygen. The alcohol and alkoxy species may be adsorbed on Lewis acid sites or other defect sites and the proton adsorbs on a lattice oxygen. Desorption of alcohol may occur via the reverse reactions:

$$\mathrm{ROH(a)} \rightarrow \mathrm{ROH(g)} \quad (3)$$

$$\mathrm{RO(a)} + \mathrm{H_2O(l)} \rightarrow \mathrm{ROH(g)} + \mathrm{O(l)} \quad (4)$$

Surface hydroxyls may also be lost by recombinative desorption to form water and oxygen surface vacancies:

$$\mathrm{H_2O(l)} + \mathrm{H_2O(l)} \rightarrow \mathrm{H_2O(g)} + V_O^{\bullet\bullet} + \mathrm{O(l)} \quad (5)$$

After desorption of alcohol at lower temperatures, by reactions 3 and 4, and loss of surface hydroxyls, via reaction 5, there is some fraction of the dissociatively adsorbed alcohol that remains as alkoxy species. These intermediates are not able to desorb as alcohol and are trapped on the surface until either C−O bond scission occurs, or a proton becomes available (e.g., from β-H elimination from a coadsorbed alkoxy species). We now consider two models that could control the coverage of alkoxy species remaining after the low-temperature desorption is complete, since these are the species that ultimately lead to alkene production.

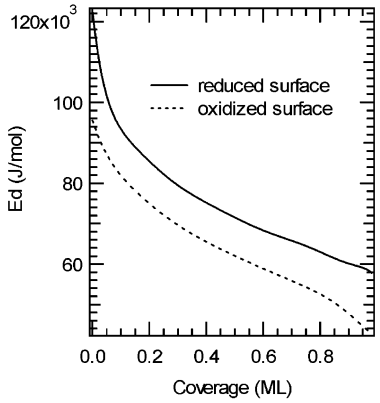

Figure 9. Relationships of desorption energy vs surface coverage which, in our Monte Carlo simulations, give rise to theoretical desorption spectra consistent with the experimental methanol desorption spectra[23] on the $WO_3(001)$ surfaces.

IV.B.1. Defect Control of Selectivity. Gamble et al.[30] proposed that the sites responsible for the ethanol dehydration reaction on the $TiO_2(110)$ surface are the bridging oxygen vacancies produced during water desorption. These vacancies, corresponding to those produced in reaction 5, bind the ethoxy intermediate much more strongly than ethoxy species adsorbed on 5-fold Ti^{4+} sites, as demonstrated by their unreactivity toward further hydroxyl exposure.[30] The surface hydroxyls are necessarily mobile, since they are removed in a recombinative desorption process as water. The coverage of ethoxy species remaining after the low-temperature desorption of ethanol (corresponding to reactions 3 and 4) was found to be approximately 25% of the original ethanol coverage.[30] Of the remaining 25% ethoxy species, approximately half desorbed as ethylene and half as ethanol after the β-H elimination step. Therefore, we first consider the role of defects on the $WO_3(001)$ surfaces.

In our previous study of methanol desorption from the $WO_3(001)$ surfaces, we interpreted the thermal desorption curves in terms of surface heterogeneity and relatively rapid diffusion of molecularly adsorbed methanol on the basis of Monte Carlo simulations.[23] The coverage-dependent desorption curves can be simulated using a distribution of adsorption site energies: the corresponding coverage-dependent desorption energies are shown in Figure 9. Because no decomposition products of methanol were observed on either the oxidized or reduced surface, the methanol desorption spectra can essentially be used as a probe of the strength of the distribution of all available adsorption sites. For the larger alcohols, the more strongly bound sites may lead to alkene production and therefore the alcohol desorption spectra only contain information about the sites that lead to associative desorption (eq 4).

The surface heterogeneity of our films can be attributed to both electronic and morphological factors. The electronic contributions to the heterogeneity of these WO_3 surfaces have been characterized experimentally by XPS and UPS.[23] The surface lattice oxygen is preferentially removed during treatment of the surface, resulting in a mixture of W^{5+} and W^{6+},[23] and probably formation of CS type line defects. Furthermore, SEM and STM images have shown that, despite being epitaxially grown, our WO_3 surfaces are heavily stepped.[41]

There is a certain fraction of the defect sites that strongly bind the alkoxy intermediate. As the temperature increases, the surface hydroxyls produced in dissociative adsorption are

removed via recombination (eq 5), while the rate of desorption of alcohol is substantially reduced (eq 4) for the strongly bound alkoxy species. This implies that the alcohol is sufficiently mobile to find these strong adsorption sites, even at low coverage. According to our Monte Carlo simulations,[23] the behavior of the coverage-dependent desorption curves, in which the trailing edge overlaps, indicates that the diffusion rate is larger than the desorption rate for water, methanol, ethanol, and 2-propanol on both the oxidized and reduced WO_3(001) surfaces. Therefore, we believe that this assumption is valid. A second assumption is that the hydroxyl groups are mobile, such that at low coverage, recombinative desorption (via eq 5) is possible. The low-temperature desorption of water from dissociatively adsorbed alcohols suggests that hydroxyls are relatively mobile, as shown in Figures 2C to 6C.

The implication of this model is that the selectivity toward dehydration should be substantially higher when the number of defects with binding energy greater than some threshold is increased. Indeed, the desorption temperature is always higher on the reduced surface than on the oxidized surface as shown in Figure 4, which implies that the distribution of binding energies is shifted to higher binding energy on the reduced surface. However, Figure 8 shows that the oxidized surface does not exhibit significantly different dehydration activity from the reduced surface for either ethanol or 2-propanol. On the oxidized surface, the ethylene yield reached 5% at high coverage. Therefore, for the distributions in Figure 9, the threshold energy corresponds to 87 kJ/mol. For the reduced surface, the fraction of sites with methanol binding energies greater than 87 kJ/mol is approximately four times larger than on the oxidized surface, which is much larger than the result presented in Figure 8B. Therefore, we find no evidence to support a defect model, at least under the low coverage conditions of the reactions on our WO_3(001) surfaces. Tanner et al.[28] suggest that the sites for dehydration are the 5-fold coordinated W^{6+} ions, and find no evidence that alkoxy species preferentially adsorb on step or other defect sites. This is consistent with our results.

IV.B.2. Selectivity Controlled by Diffusion and Surface Kinetics. As an alternative view, we suggest that the selectivity is controlled by the rates of diffusion and reaction kinetics, and that "special" defect sites are not necessarily important. The coverage of alkoxy species that remain after molecular alcohol desorption is simply the result of a competition between the kinetics of recombinative desorption of hydroxyls (eq 5) and associative desorption of hydroxyls and alkoxy species (eq 4). Whereas the rate (eq 4) for associative desorption of the alcohol may decrease from methanol to ethanol to 2-propanol, the recombinative desorption of surface hydroxyls is coverage dependent, but should not depend on the alcohol. In this model, as in the defect-controlled model, surface hydroxyls must be mobile if the rate of eq 5 is going to be competitive with the rate of associative alcohol desorption.

In our previous studies of methanol CTDS on WO_3(001) surfaces, UPS showed that methanol molecularly adsorbs on the oxidized WO_3 thin film surface and dissociates on the reduced surface.[23] The intensity of the UPS band due to the oxygen lone pair electron on the molecularly adsorbed methanol is significantly reduced. This we attribute to adsorption of methanol through a strong interaction between oxygen and a surface tungsten cation.[23] On the reduced surface, the UPS spectrum contains only three bands, which easily distinguishes methoxy species from the 5-featured spectrum of methanol.[23] However, methanol is the only species detected on both surfaces during the desorption experiments. This implies that the rate of desorption of methanol through reactions 3 or 4 is fast compared to the rate of associative desorption of hydroxyls (eq 5). For ethanol and 2-propanol, we do not have direct evidence regarding the fraction of alcohol that is associatively vs dissociatively adsorbed. It is clear from the alkene production that some fraction dissociates. For ethoxy/ethanol and isopropoxy/2-propanol, neither UPS nor vibrational spectroscopy is able to distinguish between these pairs of species, particularly in a mixture.[42,43]

On metal surfaces, the shapes of desorption spectra are frequently used to distinguish first-order desorption (eq 3) from second-order desorption (eq 4).[44−46] Figures 3A and 6A show that the desorption temperatures for ethanol and 2-propanol on the oxidized WO_3(001) surface decreased with increasing surface coverage, which is similar to the desorption of methanol on the oxidized WO_3(001) surface.[23] In particular, the desorption curves for different coverages of water and all of the alcohols have an overlapping tail on the high-temperature side. This behavior can be described, on both the oxidized and reduced surfaces, by first-order desorption kinetics with surface heterogeneity and rapid diffusion. We note that rapid diffusion of alcohols was also detected on the single-crystal WO_3(001) surface by Tanner et al.[28] A slow surface diffusion process would result in a broad desorption profile with coverage-independent desorption peak temperatures, as reported by Nelson et al., for water desorption from the α-Al_2O_3(0001) surface.[47] The broad temperature range of the desorption peaks implies a wide distribution of surface adsorption energies. Our Monte Carlo model for methanol desorption indicated that diffusion of methanol was significantly faster than desorption on both surfaces. The shape of the coverage-dependent curves was consistent with a first-order or pseudo-first-order process on the oxidized and reduced surfaces, respectively, even though methanol was molecularly adsorbed on the oxidized surface and dissociatively adsorbed on the reduced surface. Therefore, the shape of the desorption spectra are not able to determine the adsorption state.

Spitz et al.[48] showed that the relative acidity of Brønsted acids on oxide surfaces is consistent with that in aqueous solutions. The acidity of methanol, $pK_a = 15.5$, is slightly stronger than that of ethanol, $pK_a = 15.9$, and significantly stronger than that of 2-propanol, $pK_a = 17.1$. By comparison with the adsorption state of methanol on the WO_3(001) surfaces and the stronger acidity of methanol, we might expect that ethanol and 2-propanol would only adsorb molecularly on the oxidized WO_3(001) surface and would be less likely than methanol to adsorb dissociatively on the reduced surface. However, our experiments show significant amounts of alkene produced by dehydration of ethanol and 2-propanol on both the oxidized and reduced WO_3(001) surfaces (Figures 2B−6B). A detailed understanding of the acid dissociation equilibria would require information about the temperature dependence of the alcohol dissociation. We suggest that the coverage of the alkoxy which remains after dehydroxylation is a result of the stronger dispersion interactions of the larger alcohols with the surface. The higher desorption temperature of the larger alcohols leads to greater dissociation; before the alcohol desorbs, dehydroxylation occurs.

Once the surface alkoxy coverage at higher temperatures is established, the selectivity between alkene production and reaction of the hydroxyls (produced by β-H elimination) to form water or alcohol should again be dependent on the coverage and diffusion rates. When the coverage is low and hydroxyl diffusion is facile, then a larger fraction of the hydroxyls may

be lost as water, rather than through associative desorption of alcohol.

Previous studies show that the ratio of alkene to alcohol desorption at relatively high coverage in the high-temperature peak is close to 1:1 for alcohols on the $TiO_2(001)$ surface[36] and ethanol on the $TiO_2(110)$ surface.[30] Kim and Barteau[36] proposed that the formation of alkene and alcohol at high temperature is related kinetically to the β-H elimination process; the β-H abstracted from one alkoxy during formation of alkene is used to hydrogenate another alkoxy to form an alcohol molecule.

Compared with the dehydration reaction of alcohols on TiO_2 surfaces,[30,36] the yield of alcohol molecules with respect to alkene production on the WO_3 surfaces at high temperature is much lower. This observation is more prominent for 2-propanol on the WO_3 surfaces than for ethanol. Figures 5 and 6 clearly show that with the increasing production of propylene around 500 K, the desorption of 2-propanol in the corresponding temperature region does not grow significantly as observed on the $TiO_2(001)$ surface.[36] This again suggests that the rate of recombinative hydroxyl desorption is faster than associative desorption of the alcohol.

V. Conclusions

Reactions of alcohols on the reduced and oxidized $WO_3(001)$ surfaces were conducted at much lower coverages than in previous studies. Alcohols were removed from the surfaces through two channels. The first was low-temperature desorption of alcohol, with desorption spectra that indicate a broad distribution of adsorption site energies and diffusion rates that are sufficiently rapid for the alcohol to find and desorb from the most strongly bound sites. Second, alcohols were removed by dehydration to form an alkene, which desorbs at higher temperature together with water. Desorption of the alkene is a reaction-controlled process, and the rate-limiting step for dehydration of ethanol, and probably for 2-propanol, is C−O bond scission. The reduced and oxidized $WO_3(001)$ surfaces do not have significant differences in their selectivity toward the dehydration reaction. The coverage dependence of the selectivity was attributed to the role of diffusion and reaction kinetics under the low coverage conditions, which contrasts with the dehydration of alcohols on the $TiO_2(110)$[30] and $TiO_2(001)$[36] surfaces.

Acknowledgment. We acknowledge collaboration with Francois Amar and Robert Lad. We thank Robert Jackson for helpful discussions and George Bernhardt for assistance in the growth of the WO_3 films on the sapphire substrates. This work was sponsored by the Department of Navy, Naval Surface Warfare Center, Dahlgren Laboratory, Grant No. N00178-99-1-9002 and the Office of Naval Research Grant No. N00014-01-1-0921.

References and Notes

(1) Yamaguchi, T.; Tanaka, Y.; Tanabe, K. *J. Catal.* **1980**, *65*, 442.
(2) Ogata, E.; Kamiya, Y.; Ohta, N. *J. Catal.* **1973**, *29*, 296.
(3) Grunert, W.; Shpiro, E. S.; Feldhaus, R.; Anders, K.; Antoshin, G. V.; Minachev, K. M. *J. Catal.* **1987**, *107*, 522.
(4) Grunert, W.; Morke, W.; Feldhaus, R.; Anders, K. *J. Catal.* **1989**, *117*, 485.
(5) Grunert, W.; Feldhaus, R.; Anders, K.; Shpiro, E. S.; Minachev, K. M. *J. Catal.* **1989**, *120*, 444.
(6) Cantalini, C.; Sun, H. T.; Faccio, M.; Pelino, M.; Santucci, S.; Lozzi, L.; Passacantando, M. *Sens. Actuators B* **1996**, *31*, 81.
(7) Fruhberger, B.; Stirling, N.; Grillo, F. G.; Ma, S.; Ruthven, D.; Lad, R. J.; Frederick, B. G. *Sens. Actuators* **2001**, *76*, 226.
(8) Lozzi, L.; Ottaviano, L.; Passacantando, M.; Santucci, S.; Cantalini, C. *Thin Solid Films* **2001**, *391*, 224.
(9) Fruhberger, B.; Grunze, M.; Dwyer, D. J. *Sens. Actuators B* **1996**, *31*, 167.
(10) Meixner, H.; Lampe, U. *Sens. Actuators B* **1996**, *33*, 198.
(11) Solis, J. L.; Saukko, S.; Kish, L.; Granqvist, C. G.; Lantto, V. *Thin Solid Films* **2001**, *391*, 255.
(12) Salje, E.; Carley, A. F.; Roberts, M. W. *J. Solid State Chem.* **1979**, *29*, 237.
(13) Jones, F. H.; Rawlings, K.; Foord, J. S.; Cox, P. A.; Egdell, R. G.; Pethica, J. B.; Wanklyn, B. M. R. *Phys. Rev. B* **1995**, *52*, R14392.
(14) Jones, F. H.; Dixon, R. A.; Brown, A. *Surf. Sci.* **1996**, *369*, 343.
(15) Bursill, L. A.; Hyde, B. G. *J. Solid State Chem.* **1972**, *4*, 430.
(16) Sundberg, M.; Tilley, R. J. D. *J. Solid State Chem.* **1974**, *11*, 150.
(17) Pickering, R.; Tilley, R. J. D. *J. Solid State Chem.* **1976**, *16*, 247.
(18) Berak, J. M.; Sienko, M. J. *J. Solid State Chem.* **1970**, *2*, 109.
(19) Moulzolf, S. C.; LeGore, L. J.; Lad, R. J. *Thin Solid Films* **2001**, *400*, 56.
(20) Moulzolf, S. C.; Ding, S. A.; Lad, R. J. *Sens. Actuators B* **2001**, *77*, 375.
(21) Pilling, R. S.; Bernhardt, G.; Kim, C. S.; Duncan, J.; Crothers, C. B. H.; Kleinschmidt, D.; Frankel, D. J.; Lad, R. J.; Frederick, B. G. *Sens. Actuators B*, in press.
(22) Madi, A. E.; Meulendyk, B.; Pilling, R. S.; Bernhardt, G.; Lad, R. J.; Frederick, B. G. *Mater. Res. Sci.*, in press.
(23) Ma, S.; Amar, F. G.; Frederick, B. G. *J. Phys. Chem. A* **2003**, *107*, 1413.
(24) Dixon, R. A.; Williams, J. J.; Morris, D.; Rebane, J.; Jones, F. H.; Egdell, R. G.; Downes, S. W. *Surf. Sci.* **1998**, *399*, 199.
(25) Kim, K. S.; Barteau, M. A. *Surf. Sci.* **1989**, *223*, 13.
(26) Ma, S.; Jackson, R. L.; Frederick, B. G., submitted to *J. Phys. Chem.*
(27) Tanner, R. E.; Liang, Y.; Altman, E. I. *Surf. Sci.* **2002**, *506*, 251.
(28) Tanner, R. E.; Meethunkij, P.; Altman, E. I. *J. Phys. Chem. B* **2000**, *104*, 12315.
(29) Kim, K. S.; Barteau, M. A.; Farneth, W. E. *Langmuir* **1988**, *4*, 533.
(30) Gamble, L.; Jung, L. S.; Campbell, C. T. *Surf. Sci.* **1996**, *348*, 1.
(31) Jackson, R. H. Spatial Distributions and Transient Fluxes in Calibrated Thermal Desorption Spectroscopy. Ph.D., University of Maine, 2000.
(32) LeGore, L. J.; Lad, R. J.; Moulzolf, S. C.; Vetelino, J. F.; Frederick, B. G.; Kenik, E. A. *Thin Solid Films* **2002**, *406*, 79.
(33) Spectra Instruments, I. *RGA Application Bulletin # 208, Spectra Reference*.
(34) Nakao, F. *Vacuum* **1975**, *25*, 431.
(35) Nakao, F. *Vacuum* **1975**, *25*, 201.
(36) Kim, K. S.; Barteau, M. A. *J. Mol. Catal.* **1990**, *63*, 103.
(37) Machiels, C. J.; Cheng, W. H.; Chowdhry, U.; Farneth, W. E.; Hong, F.; Carron, E. M. M.; Sleight, A. W. *Appl. Catal.* **1986**, *25*, 249.
(38) Gasior, M.; Grzybowska, B. *React. Kinet. Catal. Lett.* **1986**, *32*, 281.
(39) Gercher, V. A.; Cox, D. F.; Themlin, J. M. *Surf. Sci.* **1994**, *306*, 279.
(40) Wong, G. S.; Kragten, D. D.; Vohs, J. M. *Surf. Sci.* **2000**, *452*, L293.
(41) See the STM image 7b of monoclinic WO_3 in ref 19.
(42) Bowker, M.; Madix, R. J. *Surf. Sci.* **1980**, *95*, 190.
(43) Kagel, R. O. *J. Phys. Chem.* **1967**, *71*, 844.
(44) Taylor, J. L.; Weinberg, W. H. *Surf. Sci.* **1978**, *78*, 259.
(45) Falconer, J. L.; Madix, R. J. *J. Catal.* **1977**, *48*, 262.
(46) Chan, C. M.; Aris, R.; Weinberg, W. H. *Appl. Surf. Sci.* **1978**, *1*, 360.
(47) Nelson, C. E.; Elam, J. W.; Cameron, M. A.; Tolbert, M. A.; George, S. M. *Surf. Sci.* **1998**, *416*, 341.
(48) Spitz, R. N.; Barton, J. E.; Barteau, M. A.; Staley, R. H.; Sleight, A. W. *J. Phys. Chem.* **1986**, *90*, 4067.